Effect of Annealing on the Morphology, Structure and Photoelectric Properties of AZO/Pt/FTO Trilayer Films

Li-Jing Huang · Nai-Fei Ren · Bao-Jia Li · Ming Zhou

Abstract   Aluminum-doped zinc oxide/platinum/fluorine-doped tin oxide (AZO/Pt/FTO) trilayer films were prepared by sputtering 5-nm-thick Pt layers and 150-nm-thick AZO layers in sequence on commercial FTO glass. The effects of one-step annealing and layer-by-layer annealing on the morphology, structure and photoelectric properties of the AZO/Pt/FTO trilayer films were comparatively analyzed. It is found that the both annealing approaches increased the grain size and improved the crystallinity of the films, leading to enhancement in transmittance and conductivity. However, layer-by-layer annealing led to the formation of quasi-continuous or continuous AZO layers, different from the sparsely distributed AZO particles brought about by one-step annealing, resulting in excellent optical and electrical properties. Specifically, after layer-by-layer annealing at 400 °C for both Pt and AZO layers, the AZO/Pt/FTO trilayer film showed an increase in average transmittance from 71.3% to 85.3% and a decrease in sheet resistance from 7.5 to 5.6 $\Omega/\square$, leading to the highest figure of merit of $3.64 \times 10^{-2} \ \Omega^{-1}$.

1 Introduction

Transparent conducting oxide (TCO) films, which are widely used in photoelectric device applications such as thin-film solar cells [1], flat-panel displays [2], gas sensors [3] and organic light-emitting diodes [4], have attracted tremendous academic and industrial interests in recent years. Among TCO films, tin-doped indium oxide (ITO) [5, 6], fluorine-doped tin oxide (FTO) [6] and aluminum-doped zinc oxide (AZO) [7] single-layer films hold greater promise for potential applications in solar cells because of their excellent optical and electrical properties. However, with the development of thin-film solar cells, there is an increasing requirement for the photoelectric property of single-layer TCO films. To meet this requirement, new multilayer composite films have been constantly developed for improving transparency and conductivity of single-layer films [8–10]. Many multilayer films, such as ITO/Ag/ITO [11], ITO/Pt/ITO [12], AZO/Ag/AZO [13, 14], AZO/Au/AZO [15], AZO/Al/AZO [16] and ZnO/Cu/ZnO [17, 18], have been prepared and display high transparency and low resistivity. It is noteworthy that Pt possesses the virtues of high conductivity and excellent stability, enabling it to act as an effective interlayer material for

L.-J. Huang · B.-J. Li · M. Zhou
School of Materials Science and Engineering, Jiangsu University, Zhenjiang 212013, China
e-mail: lij_huang@126.com

L.-J. Huang · N.-F. Ren · B.-J. Li · M. Zhou
Jiangsu Provincial Key Laboratory of Center for Photon Manufacturing Science and Technology, Jiangsu University, Zhenjiang 212013, China

N.-F. Ren (✉)
School of Mechanical Engineering, Jiangsu University, Zhenjiang 212013, China
e-mail: rnf_ujs@126.com

multilayer film electrodes in thin-film solar cells especially in thin-film dye-sensitized solar cells [19]. Despite the high material cost of Pt, using small amount of Pt to form a very thin Pt interlayer (several nm in thickness) can reduce the cost of the multilayer film [20].

It is well known that annealing treatment is also a conventional and effective technique to improve the photoelectric properties of TCO films. Annealing can improve crystallinity of the films through promoting grain growth and recrystallization, which will significantly affect the electrical and optical properties of TCO films [21, 22]. Tong et al. [23] reported that the electrical resistivity of AZO films annealed in hydrogen at 300 °C decreased from 9.8×10^{-4} to $3.5 \times 10^{-4} \ \Omega$ cm. Sheu et al. [24] found that the resistivity of gallium-doped ZnO (GZO) films reduced from 1.4×10^{-1} to $5.3 \times 10^{-4} \ \Omega$ cm after the films being annealed in nitrogen under the temperatures ranging from 400 to 800 °C. There are already many reports about one-step annealing approach for enhancing the photoelectric properties of multilayer TCO films [25, 26], but relatively few studies have focused on layer-by-layer annealing approach.

In this study, Pt layers and AZO layers were deposited in sequence by direct current (DC) magnetron sputtering on commercial FTO glass. Two strategies, i.e., one-step annealing and layer-by-layer annealing, were adopted to improve the photoelectric properties of the as-deposited AZO/Pt/FTO trilayer films. The effect of annealing approach on the morphology, structure and performance of the films was investigated, based on which the more effective annealing approach with the optimum annealing temperature was proposed.

2 Experimental

2.1 Pre-treatment of FTO Glass

The commercial FTO glass was cut into small pieces of 20 mm × 20 mm and cleaned with deionized water, acetone and anhydrous ethanol in an ultrasonic bath each for 10 min, followed by blowing high-purity (99.99%) nitrogen to dry the film surfaces.

2.2 Layer-by-Layer Annealing of AZO/Pt/FTO Films

Firstly, 5-nm-thick Pt layer was deposited on the pre-cleaned FTO glass by DC magnetron sputtering coater (Emitech K575X) at room temperature using a metallic Pt target (99.99% purity). The deposition chamber was evacuated to a base pressure of about 1×10^{-3} Pa, and then high-purity (99.99%) argon was introduced. The working pressure and current were 35 Pa and 60 mA, respectively. The ultimate thicknesses of the Pt layers were monitored in situ by a quartz

crystal thickness monitor. After that, the obtained Pt/FTO bilayer films were thermal annealed at 400 °C in a tube furnace (Hefei Risine CVD(Z)-06/60/3). During annealing, high-purity (99.99%) nitrogen with a constant flow rate of 10 mL/min was introduced into the furnace chamber and maintained for 20 min. Subsequently, 150-nm-thick AZO layer was deposited on the annealed Pt/FTO film by the K575X coater using a zinc–aluminum alloy target (2 wt% Al_2O_3). The working current used here was 150 mA, and the other details of deposition process were the same as described above for deposition of Pt layers. Then, the as-deposited AZO/Pt/FTO trilayer film was annealed in the tube furnace at a certain temperature (300, 400 or 500 °C) for 20 min with a nitrogen flow rate of 10 mL/min.

2.3 One-Step Annealing of AZO/Pt/FTO Films

One-step annealing of AZO/Pt/FTO trilayer film was also carried out for the purpose of comparison. Firstly, 5-nm-thick Pt layer and 150-nm-thick AZO layer were deposited in sequence on the pre-cleaned FTO glass by the K575X coater at room temperature using the metallic Pt target and zinc–aluminum alloy target, respectively. All the details of deposition process were the same as those of the AZO/Pt/FTO film prepared by layer-by-layer annealing. Then, the as-deposited AZO/Pt/FTO trilayer film was annealed in the tube furnace at a certain temperature (300, 400 or 500 °C) for 20 min with a nitrogen flow rate of 10 mL/min.

2.4 Characterization

The morphologies and thicknesses of the films were observed by a scanning electron microscope (SEM) (Carl Zeiss EVO MA10). The particle/grain size distributions and average particle/grain sizes on the film surfaces were obtained by Nano measure software. The 3D images with root-mean-square (RMS) roughnesses were scanned with an atomic force microscope (AFM) (Asylum Research MFP-3D-SA). The crystal structures of the films were examined by an X-ray diffractometer (XRD) (Rigaku D/max2500VB3+/PC) using Cu$K\alpha$ radiation ($\lambda = 0.1541$ nm) in the scan range of 2θ between 20° and 80°. The optical properties were measured by a spectrophotometer (Shimadzu UV-2550). The electrical properties were evaluated via a digital four-point probe instrument (Suzhou Baishen SX1944) and a Hall effect measurement system (Accent HL5500PC).

3 Results and Discussion

3.1 Surface Morphology of AZO/Pt/FTO Films

Figure 1 shows the surface morphology of the as-deposited AZO/Pt/FTO trilayer film. The inset in Fig. 1a

provides the particle/grain size distributions on the film surface, and the average particle/grain size was taken as the quantity to compare the grain sizes for this and subsequent films [27]. The film had a rough surface and exhibited some AZO particles with an average size of ∼160 nm, as shown in Fig. 1a. From the cross-sectional view shown in Fig. 1b, it is observed that the FTO layer exhibits the columnar growth of pyramidal shapes with a thickness of about 750 nm, and the monitored thicknesses of the Pt and AZO layers (5 and 150 nm, respectively) can be further verified.

Figure 2 shows the surface morphologies of the annealed AZO/Pt/FTO trilayer films at 300, 400 and 500 °C, respectively. The insets display the particle/grain size distributions on the corresponding film surfaces. After one-step annealing, the films were covered by sparsely distributed AZO particles rather than continuous AZO layers (Fig. 2a–c). It is unfavorable for the enhancement of the film quality, although the average particle size of AZO layer (250, 270 and 300 nm in Fig. 2a–c, respectively) becomes greater than that of the as-deposited AZO/Pt/FTO film (∼160 nm). Furthermore, the film prepared by one-step annealing at 500 °C showed some nonuniformly distributed agglomerations consisting of small particles and displayed a broad particle size distribution (Fig. 2c), which is detrimental to the optical property of the film as will be confirmed later in transmittance analysis. In the case of the layer-by-layer-annealed AZO/Pt/FTO films (Fig. 2d, e), quasi-continuous or continuous AZO layers containing densely distributed particles were obtained. Especially at 400 °C (Fig. 2e), the average particles size (∼280 nm) became greater and the particles distributed more uniform than that of the as-deposited AZO/Pt/FTO film. It may be attributed to the effective improvement in crystallinity of

the film, which will be discussed later. Uniform and larger particles were also obtained on film surfaces through layer-by-layer annealing in other reports [28]. However, when the annealing temperature increased to 500 °C, agglomerated particles with a nonuniform distribution were observed on the film surface, resulting in an average particle size of ∼320 nm (Fig. 2f). Obviously, annealing temperature was a crucial parameter that can affect the surface morphology of the films.

The 3D AFM images with a scanned region of 5 μm × 5 μm for the as-deposited AZO/Pt/FTO film and the AZO/Pt/FTO films annealed at 400 °C by the two approaches are displayed in Fig. 3. The as-deposited film exhibited a rough surface with nonuniformly distributed pyramidal particles (Fig. 3a). The surfaces of the annealed films seemed rougher and consisted of obviously enlarged particles with relative smooth edges (Fig. 3b, c). It is notable that the particles on the surface of the layer-by-layer-annealed film are larger and more densely distributed as compared to those on that of the one-step-annealed one, which is consistent with the above SEM analysis. Figure 4 gives the surface RMS roughnesses of all the films extracted from AFM data. The as-deposited AZO/Pt/FTO film had a RMS roughness of 20.13 nm. Both the one-step-annealed and layer-by-layer-annealed films showed a similar trend of variation in RMS roughness. Specifically, with increasing annealing temperature from 300 to 500 °C, the RMS roughnesses of the one-step-annealed and layer-by-layer-annealed films increased from 21.89 to 32.57 and 26.69 to 35.85 nm, respectively. Ng et al. [29] reported that when sol–gel AZO films were annealed at various temperatures from 100 to 400 °C, their RMS roughness also increased from 12 to 50 nm. The increase in RMS roughness may be ascribed to the grain growth and improved crystallinity [29, 30].
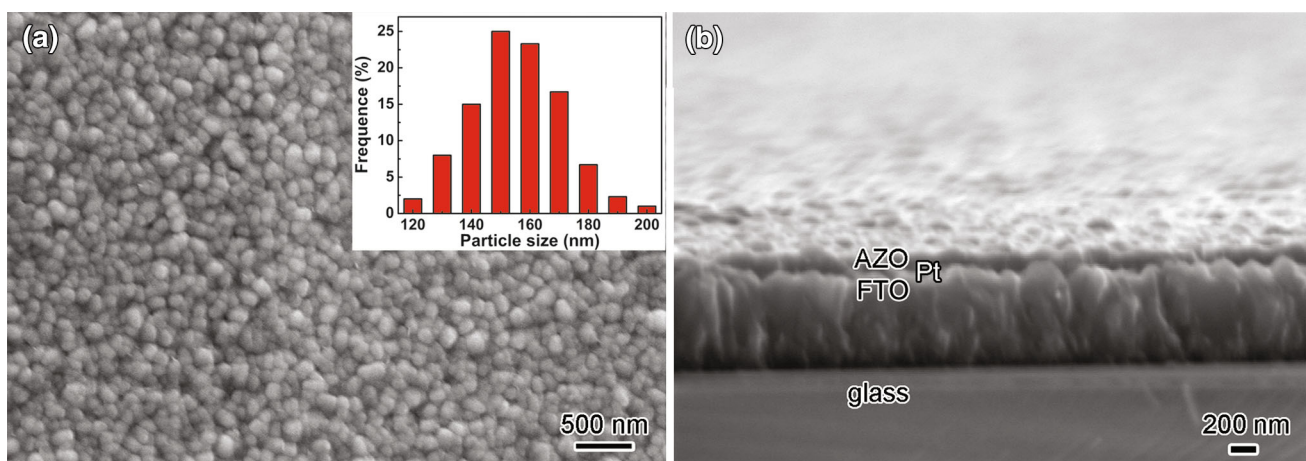

Fig. 1 SEM images of the as-deposited AZO/Pt/FTO film: **a** top view (the *inset* shows the particle size distribution on the film surface); **b** cross-sectional view
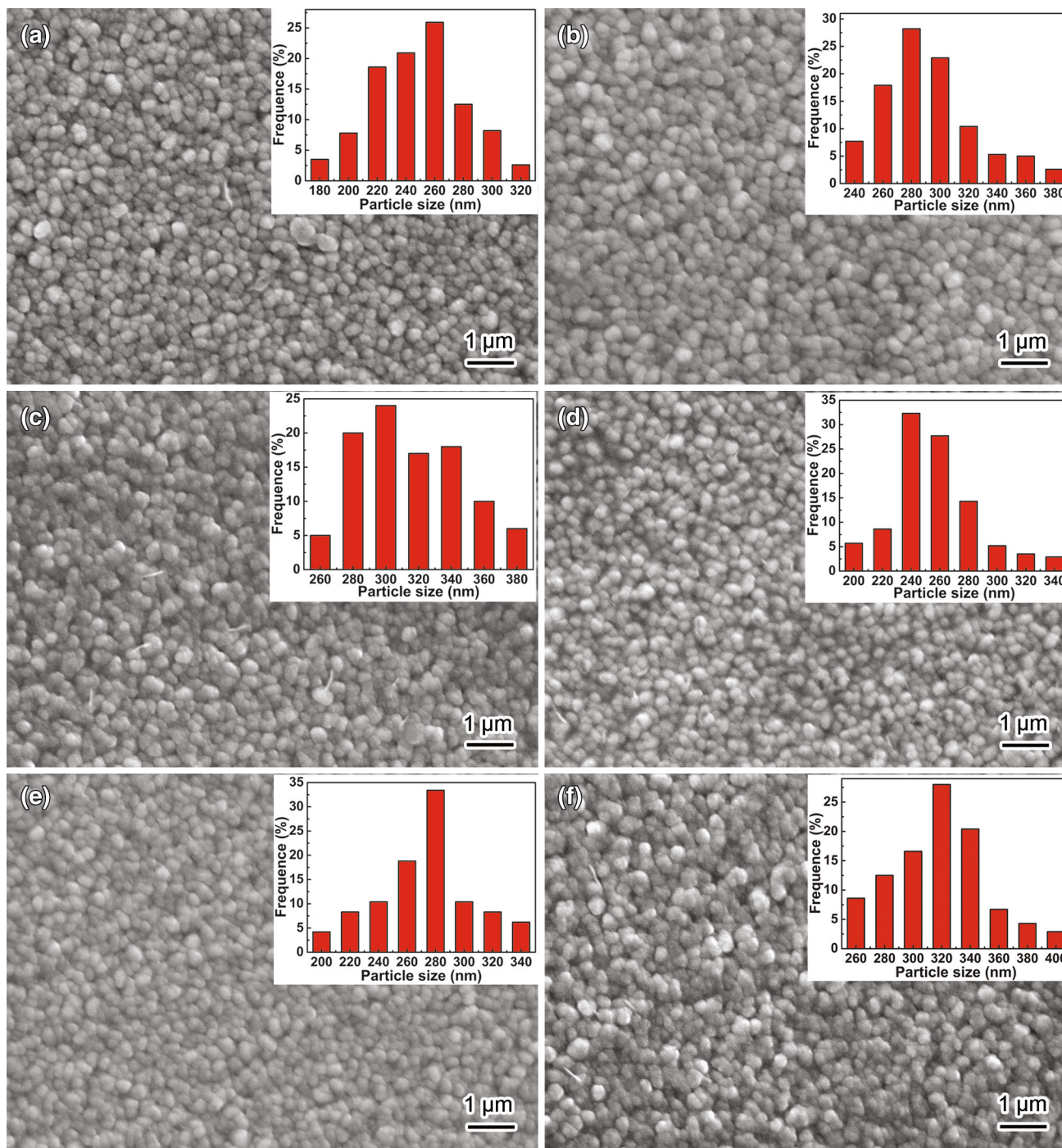
Fig. 2 SEM images of **a–c** the one-step-annealed, **d–f** the layer-by-layer-annealed AZO/Pt/FTO films at various temperatures: **a**, **d** 300 °C; **b**, **e** 400 °C; **c**, **f** 500 °C. The *insets* show the particle size distributions on the film surfaces

3.2 Structural Characterization of AZO/Pt/FTO Films

Figure 5a shows the XRD patterns of the as-deposited AZO/Pt/FTO trilayer film and the films obtained by layer-by-layer annealing under the temperatures ranging from 300 to 500 °C. It can be noticed that all the films exhibit the indexed diffraction peaks that are consistent with the standard values of the SnO_2 tetragonal structure (JCPDS no. 41-1445), the Pt face-centered cubic structure (JCPDS no. 04-0802) and the ZnO hexagonal wurtzite structure (JCPDS no. 36-1451). The strongest intensity in the SnO_2 (200) diffraction peak confirms the columnar growth of the
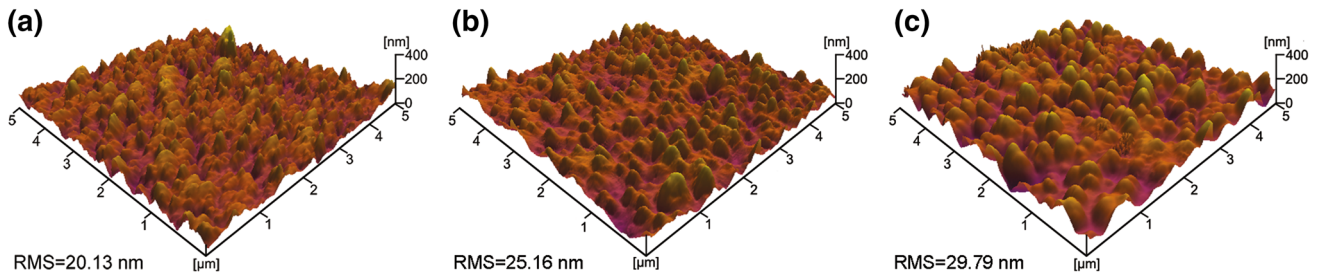
Fig. 3 AFM images of the as-deposited AZO/Pt/FTO film **a**, the one-step-annealed AZO/Pt/FTO film at 400 °C **b**, the layer-by-layer-annealed AZO/Pt/FTO film at 400 °C **c**
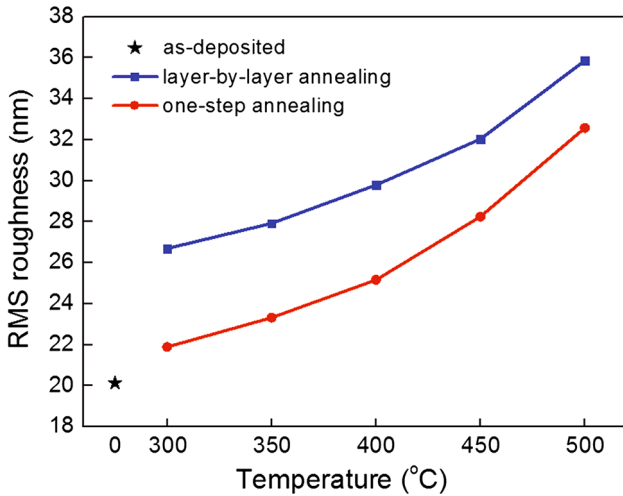

Fig. 4 Extracted surface RMS roughnesses of the as-deposited and the annealed AZO/Pt/FTO trilayer films

FTO layer [31], which has been indicated in the section of SEM analysis. Due to the annealing effect on the Pt and AZO layers, the Pt (111) peaks as well as the ZnO (100), (002) and (101) peaks of all the layer-by-layer-annealed films, as compared to those of the as-deposited film, showed slightly higher intensity and lower full width at half maximum (FWHM), indicating that crystal defects in the Pt and AZO layers were effectively reduced [32]. Moreover, with annealing temperature increasing from 300 to 500 °C, the ZnO (002) peaks showed an increase in the intensity and a decrease in the FWHM as a result of a gradual improvement in crystallinity of the films [33].

Figure 5b presents the XRD patterns of the as-deposited AZO/Pt/FTO trilayer film and the films annealed at 400 °C by layer-by-layer annealing and one-step annealing. It is found that the annealed films exhibit stronger SnO_2 (200) peaks and ZnO (002) peaks corresponding an improvement in crystallinity of the as-deposited films. Only the Pt layer in the layer-by-layer-annealed AZO/Pt/FTO film underwent direct annealing, resulting in relatively higher intensity and lower FWHM of the Pt (111) peak. In addition, compared with the as-deposited and one-step-annealed films, the SnO_2 (200) peak of the layer-by-layer-annealed film were relatively stronger and narrower, indicating higher crystallinity of the film and fewer defects in the film
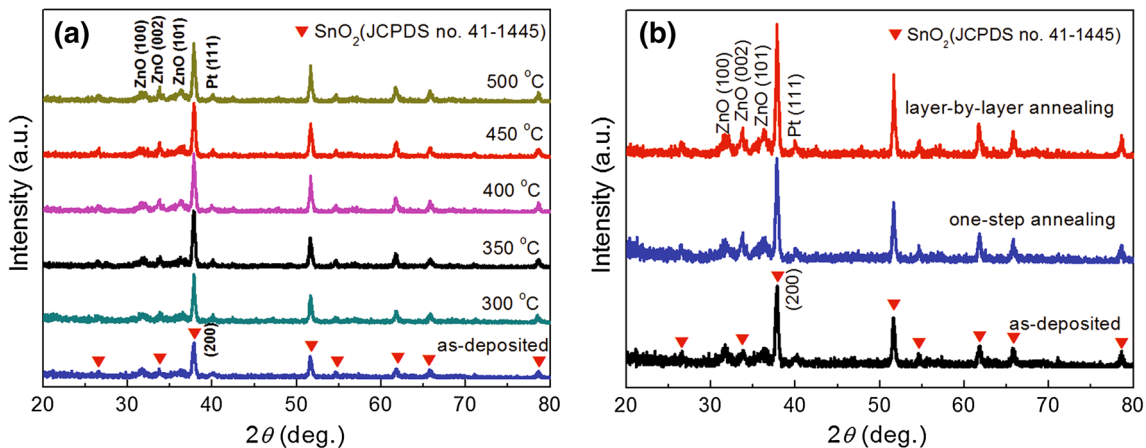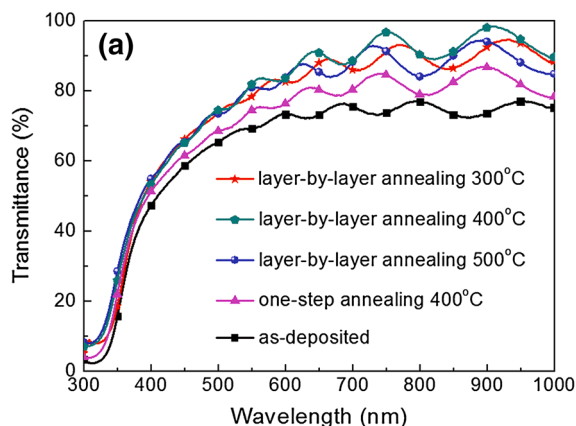

Fig. 5 a XRD patterns of the as-deposited AZO/Pt/FTO trilayer film and the layer-by-layer-annealed AZO/Pt/FTO trilayer films at various temperatures; **b** XRD patterns of the as-deposited AZO/Pt/FTO trilayer film and the AZO/Pt/FTO trilayer films annealed at 400 °C by two approaches

[32]. The twice annealing of the FTO layer in the layer-by-layer annealing process should be responsible for this result.

3.3 Photoelectric Properties of AZO/Pt/FTO Films

Figure 6a shows transmittance spectra of the as-deposited AZO/Ag/FTO trilayer film and the films annealed at different temperatures. All the films exhibited a drop-off in transmittance at shorter wavelengths that was related to the fundamental absorption caused by band-to-band transition [34]. The transmittance of the as-deposited AZO/Ag/FTO film was significantly improved after employing both layer-by-layer annealing and one-step annealing. But the increment achieved by layer-by-layer annealing was obviously greater than that by one-step annealing, which may be ascribed to the fact that the quasi-continuous or continuous AZO layer can suppress the total internal reflection in the Pt and FTO layers [35, 36]. It is noteworthy that the absorption edges for all the annealed films shifted to the shorter wavelength side compared with the as-deposited one, and the wavelengths of the absorption edges for the layer-by-layer-annealed films decreased with an increase in annealing temperature, similar to the results for AZO films reported by Ali et al. [34]. According to previous researches, the blueshift of absorption edge should be due to the improved crystallinity and the increased carrier concentration (called as Burstein–Moss effect) [37, 38]. Figure 7 presents the dependence of the carrier concentration of all the AZO/Ag/FTO trilayer films on annealing temperature. It is seen that the carrier concentrations of both the one-step-annealed and layer-by-layer-annealed films are higher than that of the as-deposited one, and increase obviously with increasing annealing temperature. These provide evidence for the above explanation.

The average optical transmittance in the wavelength range of 400–1,000 nm of the films is illustrated in Fig. 6b.

The average transmittance of the as-deposited AZO/Pt/FTO trilayer film was about 71.3%. After layer-by-layer annealing, the average transmittance greatly increased from 80.2% to 85.3% with increasing annealing temperature from 300 to 400 °C, and then dropped to 82.6% with increasing annealing temperature to 500 °C. For the one-step-annealed AZO/Pt/FTO trilayer films, the average transmittance increased to a maximum of 77.3% at an annealing temperature of 400 °C and then gently decreased to 75.3% with increasing annealing temperature to 500 °C. No matter what annealing methods and annealing temperatures are adopted, the increase in particle/grain size and the improvement in crystallinity lead to less grain boundaries and reduce the light scattering at the grain boundaries, resulting in the enhancement of the transmittance [39]. The decrease in average transmittance of the films that annealed at a temperature higher than 400 °C may be related to the nonuniformly distributed agglomerated particles that were observed on the film surfaces (Fig. 2c, f), since the nonuniformity of particles/grains can bring about the increases
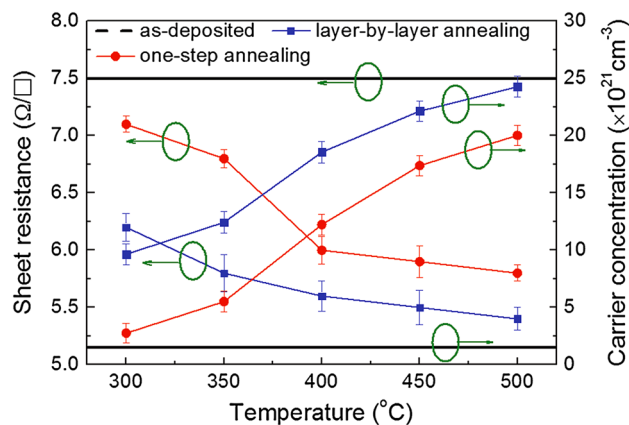
Fig. 7 Sheet resistances and carrier concentrations of the as-deposited and the annealed AZO/Pt/FTO trilayer films
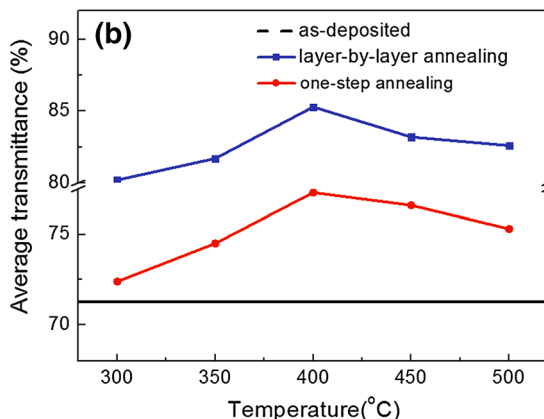
Fig. 6 **a** Transmittance spectra and **b** average transmittances (400–1,000 nm) of the as-deposited and the annealed AZO/Pt/FTO trilayer films

in scattering and absorption of light in the film, and therefore, reduce the transparency of the film [40, 41].

The dependence of sheet resistance on the annealing temperature for the annealed AZO/Pt/FTO trilayer films is also shown in Fig. 7. Compared with that of the as-deposited AZO/Pt/FTO film (7.5 $\Omega/\square$), the sheet resistances of all the annealed AZO/Pt/FTO trilayer films were relatively low. Annealing does not only eliminate parts of the crystal defects in the films (as indicated in XRD analysis), it also enhances carrier mobility and reduces carrier scattering at the grain boundaries by increasing grain size [42, 43]. All these should be responsible for the improvement in conductivity of the films. The sheet resistance of the one-step-annealed films decreased from 7.1 to 5.8 $\Omega/\square$ with increasing annealing temperature from 300 to 500 °C. The sheet resistance of the layer-by-layer-annealed films decreased from 6.2 to 5.4 $\Omega/\square$ with the same change in annealing temperature. However, at the same annealing temperature, the sheet resistance of the film prepared by layer-by-layer annealing was obviously lower than that of by one-step annealing (e.g., 5.6 vs. 6.0 $\Omega/\square$, at 400 °C), which may be attributed to the greater grain size and fewer defects in the former film. In addition, the blueshift of absorption edge in the transmittance spectra (Fig. 6a) that corresponds to the increase in carrier concentration may be conducive to improving conductivity of the films [44], which can further explain this result.

The quality of the trilayer films can be determined by a figure of merit (F_{TC}) defined as $F_{TC} = T^{10}/R_S$ [45], where T is the average transmittance in the wavelength range of 400–1,000 nm and R_S is the sheet resistance. The figures of merit of the as-deposited and annealed AZO/Pt/FTO trilayer films in our work are shown in Fig. 8. The figure of merit of the as-deposited film was only $0.45 \times 10^{-2} \, \Omega^{-1}$ and was enhanced by both layer-by-layer and one-step annealing. The film prepared by layer-by-layer annealing at 400 °C had the highest figure of merit of $3.64 \times 10^{-2} \, \Omega^{-1}$, almost three times higher than that of the corresponding one-step-annealed film ($1.27 \times 10^{-2} \, \Omega^{-1}$). By adopting the same definition for T, Dimopoulos et al. [15] calculated F_{TC} for AZO/Au/AZO trilayer films and obtained the best value of $6.9 \times 10^{-3} \, \Omega^{-1}$, significantly lower than that is presented here. Sutthana et al. [14] and Lin et al. [16] took the average transmittance in the visible range as T, yielding the highest F_{TC} of $6.9 \times 10^{-4} \, \Omega^{-1}$ for AZO/Ag/AZO films and $1.94 \times 10^{-2} \, \Omega^{-1}$ for AZO/Al/AZO films, respectively. These are uncomparable to the corresponding value of $2.42 \times 10^{-2} \, \Omega^{-1}$ for the AZO/Pt/FTO film in this study. In addition, Sahu and Huang [18] used the maximum T value for the calculation of F_{TC} for ZnO/Cu/ZnO multilayer film. In comparison, the highest F_{TC} calculated by using the maximum T in our work is $15.31 \times 10^{-2} \, \Omega^{-1}$ and outperforms their result ($1.97 \times 10^{-2} \, \Omega^{-1}$). Our work indicates that layer-by-layer annealing, rather than one-step annealing, is
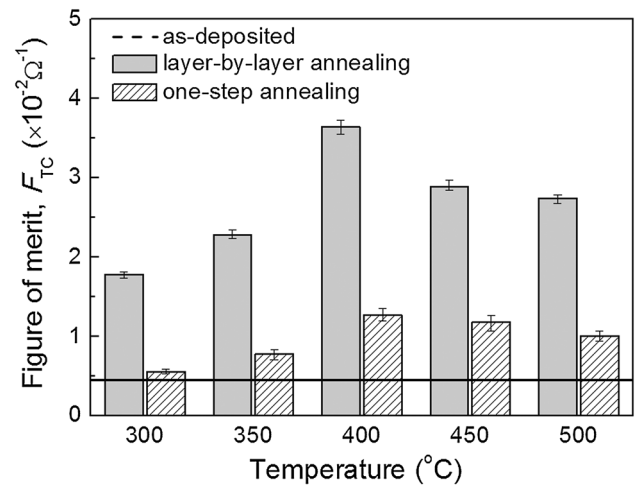

Fig. 8 Figures of merit of the as-deposited and the annealed AZO/Pt/FTO trilayer films

more effective for improving the quality of multilayer films. More importantly, the AZO/Pt/FTO trilayer films with higher quality obtained by layer-by-layer annealing are quite valuable for window electrodes in various photovoltaic applications particularly in dye-sensitized solar cells.

4 Conclusions

In summary, AZO/Pt/FTO trilayer films were prepared through coating commercial FTO glass with 5-nm-thick Pt layers and 150-nm-thick AZO layers by DC magnetron sputtering. The as-formed AZO/Pt/FTO trilayer films, which possessed an average transmittance of 71.3%, a sheet resistance of 7.5 $\Omega/\square$ and a figure of merit of $0.45 \times 10^{-2} \, \Omega^{-1}$, were treated by one-step annealing and layer-by-layer annealing. In the present work, all the annealed films exhibited an increase in the grain size and an improvement in the crystallinity, thereby achieving the enhancement in photoelectric properties. However, one-step annealing led to the formation of sparsely distributed AZO particles, resulting in relatively smaller increment in transmittance and conductivity. The layer-by-layer-annealed films were covered with quasi-continuous or continuous AZO layers and exhibited excellent optical and electrical properties. In particular, the film treated by layer-by-layer annealing at 400 °C had the highest figure of merit of $3.64 \times 10^{-2} \, \Omega^{-1}$ with an average transmittance of 85.3% and a sheet resistance of 5.6 $\Omega/\square$. The results indicate that layer-by-layer annealing can more effectively improve the photoelectric properties of multilayer films.

References

[1] S. Ito, T.N. Murakami, P. Liska, C. Grätzel, M.K. Nazeeruddin, M. Grätze, Thin Solid Films **516**, 4613 (2008)

[2] G.S. Chae, Jpn. J. Appl. Phys. **40**, 1282 (2001)

[3] T. Miyata, T. Hikosaka, T. Minami, Sens. Actuators, B **69**, 16 (2000)

[4] S.B. Kang, J.W. Lim, S. Lee, J.J. Kim, H.K. Kim, J. Phys. D **45**, 325102 (2012)

[5] S.I. Na, S.S. Kim, J. Jo, D.Y. Kim, Adv. Mater. **20**, 4061 (2008)

[6] S. Cornelia, G. Constantin, A. Stefan, Thin Solid Films **519**, 595 (2010)

[7] J.W. Leem, D.H. Joo, J.S. Yu, Sol. Energy Mater. Sol. Cells **95**, 2221 (2011)

[8] A. Zyoud, I. Saa'deddin, S. Khudruj, Z.M. Hawash, D.H. Park, G. Campet, H.S. Hilal, Solid State Sci. **18**, 83 (2013)

[9] J.C. Berne'de, L. Cattin, M. Morsli, Y. Berredjem, Sol. Energy Mater. Sol. Cells **92**, 1508 (2008)

[10] D.S. Ghosh, T.L. Chen, N. Formica, J. Hwang, I. Bruder, V. Pruneri, Sol. Energy Mater. Sol. Cells **107**, 338 (2012)

[11] K.H. Choi, J.Y. Kim, Y.S. Lee, H.J. Kim, Thin Solid Films **341**, 152 (1999)

[12] J.I. Choi, J.Y. Lee, J.H. Park, J.H. Chae, H.J. Park, D. Kim, J. Phys. Chem. Solids **70**, 272 (2009)

[13] F.S. Li, Y.Z. Zhang, C.X. Wu, Z.X. Lin, B.B. Zhang, T.L. Guo, Vacuum **86**, 1895 (2012)

[14] S. Sutthana, N. Hongsith, S. Choopun, Curr. Appl. Phys. **10**, 813 (2010)

[15] T. Dimopoulos, G.Z. Radnoczi, B. Pécz, H. Brückl, Thin Solid Films **519**, 1470 (2010)

[16] Y.S. Lin, W.C. Tseng, J. Electron. Mater. **41**, 437 (2012)

[17] K. Sivaramakrishnan, T.L. Alford, Appl. Phys. Lett. **94**, 052104 (2009)

[18] D.R. Sahu, J.L. Huang, Appl. Surf. Sci. **253**, 827 (2006)

[19] H. Kim, G. Veerappan, J.H. Park, Electrochim. Acta **137**, 164 (2014)

[20] C.C. Yang, H.Q. Zhang, Y.R. Zheng, Curr. Appl. Phys. **11**, S147 (2011)

[21] B.L. Zhu, X.H. Sun, X.Z. Zhao, F.H. Su, G.H. Li, X.G. Wu, J. Wu, R. Wu, J. Liu, Vacuum **82**, 495 (2008)

[22] C. Guillén, J. Herrero, Vacuum **84**, 924 (2010)

[23] H. Tong, Z.H. Deng, Z.H. Liu, C.G. Huang, J.Q. Huang, H. Lan, C. Wang, Y.G. Cao, Appl. Surf. Sci. **257**, 4906 (2011)

[24] J.K. Sheu, K.W. Shu, M.L. Lee, C.J. Tun, G.C. Chi, J. Electrochem. Soc. **154**, 521 (2007)

[25] H. Kermani, H.R. Fallah, M. Hajimahmoodzadeh, Phys. E **47**, 303 (2013)

[26] A. Kim, Y. Won, K. Woo, C.H. Kim, J. Moon, ACS Nano **7**, 1081 (2013)

[27] Y. Yang, P. Lan, M. Wang, T. Wei, R. Tan, W. Song, Nanoscale Res. Lett. **7**, 481-1 (2012)

[28] H.C. Wang, C.H. Liao, Y.L. Chue, C.C. Lai, P.C. Chou, S.Y. Ting, Opt. Mater. Express **3**, 295 (2013)

[29] Z.N. Ng, K.Y. Chan, T. Tohsophon, Appl. Surf. Sci. **258**, 9604 (2012)

[30] H.M. Lee, Y.J. Lee, I.S. Kim, M.S. Kang, S.B. Heo, Y.S. Kim, D. Kim, Vacuum **86**, 1494 (2012)

[31] C. Agashe, J. Hüpkes, G. Schöpe, M. Berginski, Sol. Energy Mater. Sol. Cells **93**, 1256 (2009)

[32] L.J. Huang, N.F. Ren, B.J. Li, M. Zhou, Mater. Lett. **116**, 405 (2014)

[33] Z.Z. Zhi, Y.C. Liu, B.S. Li, X.T. Zhang, Y.M. Lu, D.Z. Shen, X.W. Fan, J. Phys. D **36**, 719 (2003)

[34] H.M. Ali, M.M. Abd El-Raheem, N.M. Megahed, H.A. Mohamed, J. Phys. Chem. Solids **67**, 1823 (2006)

[35] J.H. Lim, K.H. Lee, D.C. Lim, J. Korean Phys. Soc. **57**, 1229 (2010)

[36] N.F. Ren, L.J. Huang, M. Zhou, B.J. Li, Ceram. Int. **40**, 8693 (2014)

[37] S. Suzuki, T. Miyata, M. Ishii, T. Minami, Thin Solid Films **434**, 14 (2003)

[38] H. Kim, J.S. Horwitz, S.B. Qadri, D.B. Chrisey, Thin Solid Films **420–421**, 107 (2002)

[39] R.J. Winfield, L.H.K. Koh, S. O'Brien, G.M. Crean, Appl. Surf. Sci. **254**, 855 (2007)

[40] M. Hezam, N. Tabet, A. Mekki, Thin Solid Films **518**, 161 (2010)

[41] B.R. Kumar, T.S. Rao, J. Optoelectron. Biomed. Mater. **4**, 35 (2012)

[42] S. Lee, J. Seong, D.Y. Kim, J. Korean Phys. Soc. **56**, 782 (2010)

[43] B.J. Li, L.J. Huang, M. Zhou, N.F. Ren, B. Wu, Ceram. Int. **40**, 1627 (2014)

[44] G. Fang, D. Li, B.L. Yao, Vacuum **68**, 363 (2002)

[45] M.S. Kim, D.Y. Kim, M.Y. Cho, G. Nam, S. Kim, D.Y. Lee, S.O. Kim, J.Y. Leem, Vacuum **86**, 1373 (2012)